CHEMISTRY
A European Journal

A Journal of
ChemPubSoc Europe

Accepted Article

Title: Mild homogeneous synthesis of gold nanoparticles through the epoxide route: kinetics, mechanisms and related one-pot composites

Authors: Matias Jobbagy, Víctor Oestreicher, Cristián Huck-Iriart, Galo Soler-Illia, and Paula C. Angelomé

To be cited as: *Chem. Eur. J.* 10.1002/chem.201905335

Link to VoR: http://dx.doi.org/10.1002/chem.201905335

Supported by
ACES

WILEY-VCH

10.1002/chem.201905335

Mild homogeneous synthesis of gold nanoparticles through the epoxide route: kinetics, mechanisms and related *one-pot* composites

Víctor Oestreicher,[*a, b, #] Cristián Huck-Iriart,[c] Galo Soler-Illia,[a]
Paula C. Angelomé[b] and Matías Jobbágy[*d]

[a]Instituto de Nanosistemas, UNSAM, CONICET, 25 de mayo 1021, San Martín (1650), Buenos Aires, Argentina.; E-mail: victor.oestreicher@uv.es

[b]Gerencia Química & Instituto de Nanociencia y Nanotecnología, Centro Atómico Constituyentes, Comisión Nacional de Energía Atómica, CONICET, Av. Gral. Paz 1499, San Martín (B1650KNA), Buenos Aires, Argentina.

[c]Escuela de Ciencia y Tecnología, UNSAM, CONICET, 25 de mayo 1650, San Martín (1650), Buenos Aires, Argentina.

[d]Departamento de Química Inorgánica, Analítica y Química Física/INQUIMAE, Facultad de Ciencias Exactas y Naturales, Universidad de Buenos Aires, Ciudad Universitaria, Pab. II, Buenos Aires (C1428EHA) Argentina; E-mail: jobbag@qi.fcen.uba.ar

[#]Current address: Instituto de Ciencia Molecular (ICMol), Universidad de Valencia, Catedrático José Betrán 2, 46980, Paterna, Valencia, Spain

A new one-pot room temperature homogeneous methodology to obtain Au nanoparticles (AuNP), based on the epoxide route is presented. The proposed method takes advantage of the homogenous generation of OH^- moieties driven by epoxide ring-opening, mediated by chloride nucleophilic attack. Once reached an alkaline condition, the reducing media allows the quantitative formation of AuNP under a well-defined kinetic control. A stabilizing agent, as PVP or CTAC, is required to maintain the AuNP stable; meanwhile their presence dramatically affects the reduction kinetics and pathway, as demonstrated by the evolution of the UV-Vis spectra, SAXS patterns and pH along the reaction. In the presence of PVP-10k, nanogold spheroids are obtained following a similar reduction mechanism as the observed for control experiments in the absence of PVP. However, If CTAC is employed, a stable complex with Au(III) is formed, leading to a different reaction pathway and resulting in ellipsoidal-like shaped AuNP. Moreover, the proposed methodology allows stabilize the growing AuNP, by coupling their formation with non-alkoxidic sol-gel reactions, leading to nanocomposite gels with embedded metallic nanoparticles. The epoxide route thus offers a versatile scenario for the one-pot preparation of novel metal nanoparticles-inorganic/hybrid matrices nanocomposites with valuable optical properties.

Introduction

Gold nanoparticles (AuNP) are among the most studied noble metal nanoparticles due to their key role in fundamental and applied nanoscience.[1] Several morphologies and sizes could be obtained nowadays, such as spheres, rods, triangles, bipyramids, among others.[2,3,4] This wide variety of AuNP with well controlled sizes and shapes was exploited for the production of new optical[5,6] and Surface Enhanced Raman Spectroscopy[7,8] based sensors and more efficient catalysts[9,10,11,12] and for innovative medical[13,14] and biological applications.[15,16] Depending on the chosen applications, the nanoparticles can be used directly in solution, forming arrays onto surfaces[17] or embedded in inorganic or polymeric matrices, in nanocomposites.[18,19,10,12] The reported methods to obtain such nanoparticles typically involve the direct mixture of the reagents and can be divided into two families: one-step synthesis or seed-mediated approaches.[2] While the former are inherently easier to implement, the latter offer a more accurate textural control over the final nanoparticles, achieving sophisticated morphologies. Nowadays much effort is focused on improving the performance of *one-pot* routes, elucidating the role of the most relevant and eventually hidden experimental variables. Perhaps the most popular one-step approach is the Turkevich method,[20] which consists in adding a reducing agent (sodium citrate) adjusted at a suitable pH value, to a boiling tetrachloroauric acid solution. In this case, in the starting reagent's mixture Au(III) ions are instantly exposed to a quantitative driving force for their reduction. Spheroidal AuNP with diameter around 15 nm are obtained by this means. Even this relatively simple synthesis, that has been tested for more than 60 years, is still being revisited in the recent literature, with the objective of controlling size reproducibility and monodispersity of the resulting AuNP.[21,22] For example, Ojea-Jiménez *et al.*[23] have demonstrated that the mixing sequence of the reagents has an effect over the AuNP size and morphology. Also, Schulz *et al.*[24] demonstrated that there is an optimum pH value that gives rise to uniform and monodisperse AuNP. In the same sense, Kettermann *et al.*[25] studied the Turkevich method in great detail alerting about the influence of the resulting pH solution over the size and polydispersion of the obtained AuNP. On recent years, milder reducing agents such as alcohols and polyols gained increasing attention, since they offer a proper reactivity in aqueous media, defining a highly eco-friendly synthesis.[26,27,28,29,30] However, the inherently inconvenient scenario, related to the mixing sequence of the reagents and pH optimization, still remains.[31]

Most of these inherent drawbacks related to adding and mixing solutions that are dramatically apart from chemical equilibrium, can be solved employing homogeneous synthesis methods. In those ones, the chemical driving force for particle's formation is activated after the reagent's mixture, typically by temperature increment or the *in situ* generation of one of the reagents. This approach ensures that both the nucleation and growth of the particles take place in the absence of any compositional inhomogeneity in the solution.

In this context, the *in situ* alkalinization of a solution containing an Au(III) precursors in the presence of a reducing agent, which can only effectively react under alkaline conditions, can fulfil the requirements for a

10.1002/chem.201905335

one-pot synthesis on a homogenous basis.

In recent years, the epoxide route has demonstrated a great versatility to drive the homogenous alkalinization of acidic solutions at room temperature. Nucleophilic attack over epoxides, typically driven by chloride,[32] is able to drive the precipitation of several inorganic materials with an exquisite textural control,[33,34] including metal (hydro)oxides,[35] layered basic salts,[36,37] layered double hydroxides,[32,38,39] silicates,[40] phosphates,[41] and more recently hybrid layered structures and metal organic frameworks[42], in all the cases in a *one-pot* approach at room temperature conditions. In parallel, coupled with the alkalinisation process, this *in situ* method releases diols to the media, resulting from the partial hydrolysis of the epoxide. Taking into account the mild and controllable release of diol and hydroxide to the reaction medium, the epoxide route can potentially drive metallic gold formation, on the basis of an irreversible redox process.

The present work introduces the homogeneous reduction of $HAuCl_4$ into metallic AuNP, through the epoxide route for the very first time. The homogeneous growth mechanism is comprehensively studied by means of *in situ* UV-Vis spectroscopy, SAXS and pH evolution characterization, alerting about the non-innocent role of stabilizing agent on the chemical speciation of Au(III) and its reactivity. In addition, we present a particular application in which the reduction process is sequentially coupled with a non-alkoxidic sol-gel process, leading to building nanocomposites (AuNP at inorganic hydrogels) of high optical quality on *one-pot* basis. This work paves the way towards the generation of a wide variety of AuNP and composites by *one-pot* room temperature homogenous methods. Moreover, it demonstrates the feasibility of using such methods to perform careful physicochemical characterization of the AuNP formation process.

Experimental results

1. Synthesis feasibility. The alkalinization method based on the epoxide route consists in the nucleophilic attack over an electrophilic carbon belonging to the epoxide ring.[32] This reaction typically carried out by chloride anions, added as KCl, results in the epoxide's ring-opening of glycidol (or Gly) in the present case, and chlorohydrines formation (see Scheme 1, reactions 1 and 2). Nevertheless, aqueous media itself is able to decompose Gly through a hydrolytic attack, resulting in the formation of glycerol (see Scheme 1, reaction 3). This side reaction, that cannot contribute to the net alkalinization, is favoured either in acid or alkaline media.

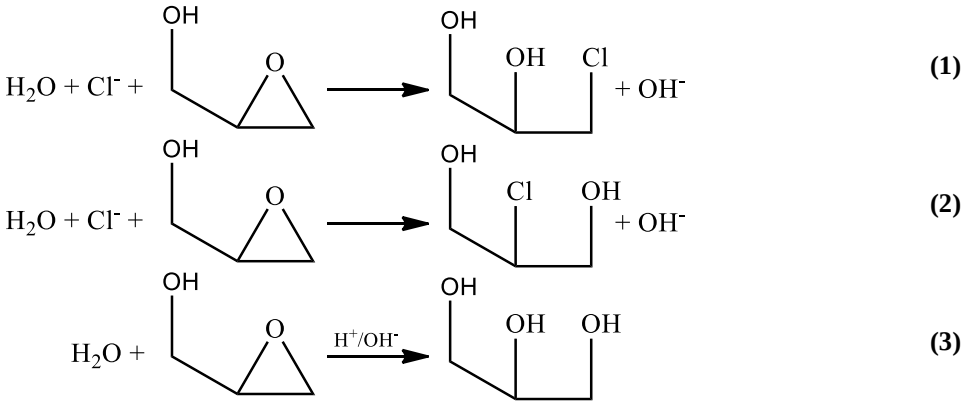

Scheme 1. Ring rupture reaction of glycidol in aqueous media: chloride attack with chlorohydrin formation and net alkalinization (reactions 1 and 2) or epoxide hydrolysis (acid or alkali catalysed glycerol formation, reaction 3).

In order to evaluate the feasibility of the epoxide route to drive Au(III) reduction, $HAuCl_4$, KCl and the main reducing agent, glycerol, were mixed at room temperature (see Experimental Details), on the basis of typical AuNP synthesis procedures through polyol reduction. No signs of reduction were observed when the $HAuCl_4$ (acid precursor) and KCl were mixed in the presence of glycerol; alkaline media (KOH) in the absence of glycerol gave similar results. Quantitative reduction took place once this solution was mixed in alkaline conditions, confirming the inherent reducing ability of polyols at room temperature, once pH is raised to the proper value.[26,27,28,29,30]

Once the potential ability of Gly to drive the homogenous reduction of Au(III) was established, the experimental conditions were screened in order to ensure the quantitative formation of metallic nanoparticles, on the basis of the inherent reactivity of these reagents.[32] When Gly (responsible of the alkalinization reaction and polyol generation, see Scheme 1) was added, the initial $HAuCl_4$ yellow solution, containing chloride anions, turned colourless and then reddish, indicating quantitative reduction of Au(III) into Au(I) subsequently followed by Au nanoparticle formation. Nevertheless, the obtained nanoparticles tended to aggregate and precipitate along their growth, as presented in Figure 1-A; UV-Vis spectra also confirmed this naked eye observation (see Figure S1). This result suggests that products of Gly ring's opening, glycerol and both chlorohydrin isomers,

10.1002/chem.201905335

or their resulting oxidized forms, are not effective stabilizing agents, hence AuNP tend to agglomerate due the high ionic strength given by at least 100 mM of K^+. Aiming at improving the epoxide route as a synthetic method, already proved by the sequential reduction of Au(III)-Au(I)-Au(0), a stabilizing agent must be used in order to avoid aggregation. Polyvinylpyrrolidone, MW=10000 g/mol (PVP−10k), and cetyltrimethylammonium chloride (CTAC) were chosen as polymeric and cationic stabilizing agents, respectively. In these samples, Gly was added to solutions containing $HAuCl_4$, KCl and PVP−10k or CTAC at room temperature; none of these additives affects the alkalinization rate of chloride-Gly reaction (see Figure S2). An analogous quantitative reduction sequence was observed, while reddish AuNP suspensions are obtained, that remain stable for months (Figure 1-B and 1-C).

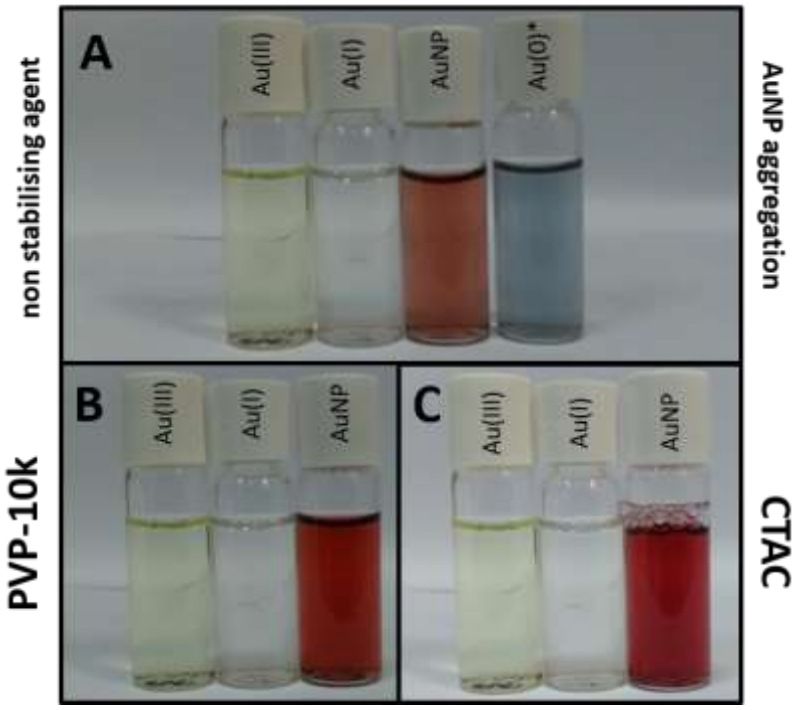

Figure 1. Images of representative samples belonging to the different states reached along the reaction employing initial concentrations of: $[HAuCl_4]$ = 0.5 mM; $[Cl^-]$ = 100 mM; [Gly] = 2500 mM without stabilizing agent (A) and with [PVP 10k] = 0.11 mM (B); or [CTAC]= 10 mM (C) at 25 °C.

TEM inspection over the stabilized AuNP is presented in Figure 2. Morphological characterization by TEM performed over more than 100 nanoparticles of both samples allows to confirm the obtention of spheroidal nanoparticles with a diameter of 10 ± 2 nm and 14 ± 3 nm for PVP−10k and CTAC, respectively. These experiments demonstrate the feasibility of the proposed synthetic methodology to obtain spheroidal AuNP, exclusively, in a homogeneous *one-pot* reaction at room temperature.

10.1002/chem.201905335

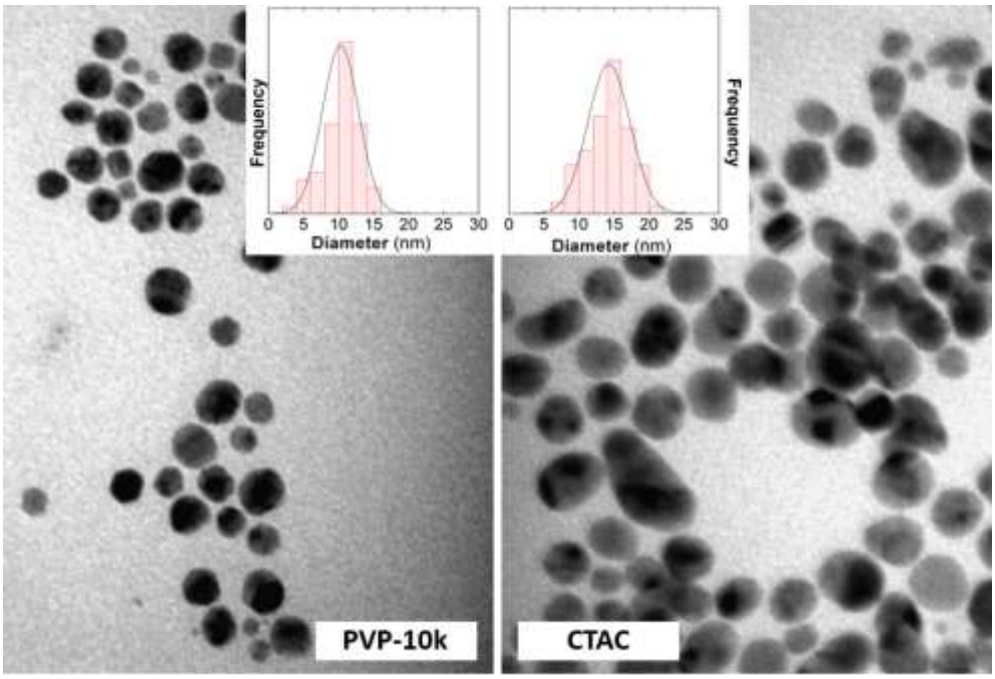

Figure 2. TEM images of AuNP obtained employing initial concentrations of: [$HAuCl_4$] = 0:5 mM; [Cl^-] = 100 mM; [Gly] = 2500 mM and [PVP-10k] = 0:11 mM (left); or [CTAC] = 10 mM (right) at 25 ^oC; scale bar represents 50 nm for both images. Inset: Size distribution estimated over more than 100 nanoparticles.

2. Kinetics of Au(III) reduction and the effect of molecular stabilizing agents on growth mechanism. In order to perform a further inspection over the main parameters that govern the alkalinization reaction, the variation of both chloride and glycidol concentrations could be explored. Chloride concentration modulates both gold reduction potential (see Figure S3) and the alkalinization (Reactions 1 and 2, Scheme 1) *vs.* hydrolysis (Reaction 3, Scheme 1) rates.[32] In the present approach, in order to have a simplified kinetics screening, only glycidol concentration was explored as the experimental parameter to regulate the reaction rate. A set of experiments screening initial glycidol concentrations from 250 mM to 5000 mM were carried out in the presence of each one of the stabilizing agents. Under all the evaluated conditions stable AuNP were obtained. Reaction time decreases when glycidol concentration increases as expected according to the alkalinization rate (eq. 4):

$$v_{OH^-} = \frac{d[OH^-]}{dt} = k[Cl^-][Gly] \quad (4)$$

Reaction completion can be tuned from 30 minutes to one day, and from 10 minutes to a couple of hours when PVP−10k or CTAC are used as stabilizing agents, respectively. For each condition, experiments performed using CTAC were always faster than PVP−10k ones. Figure S4 depicts UV-Vis spectra of the prepared samples, with its Localized Surface Plasmon Resonance (LSPR) band position. A clear trend for PVP−10k experiment is observed. LSPR band position shifts from

10.1002/chem.201905335

~ 530 nm to ~ 510 nm with glycidol concentration increment. However, for CTAC ones, the LSPR band position remains practically invariant around 523±1 nm under the same scenario. In all the experiments, the absorbance at 400 nm reaches the expected value of 1.20 ± 0.05 indicating a quantitative reduction of Au(III) into metallic nanoparticles.[43] These experiments demonstrate that AuNP can be obtained in a wide range of experimental conditions, and its characteristics depends on both glycidol concentration and the chosen stabilizing agent. In order to understand the reduction sequence (already observed by naked eye – Figure 1) and how the alkalinization method controls the reduction process, detailed kinetic studies were performed under a given glycidol to Au(III) ratio. Figure 3 depicts the characteristic evolution of the UV-Vis spectra recorded during the reaction in the presence of each one of the chosen stabilizing agents, PVP−10k and CTAC; a control experiment in the absence of stabilizer is also presented. The inspection around 275−375 nm gives information about the presence of Au(III) complexes,[44] while the absorption bands in the 375 −825 nm region give information about LSPR band of AuNP, whose position is related to their shape and size.[45]

10.1002/chem.201905335

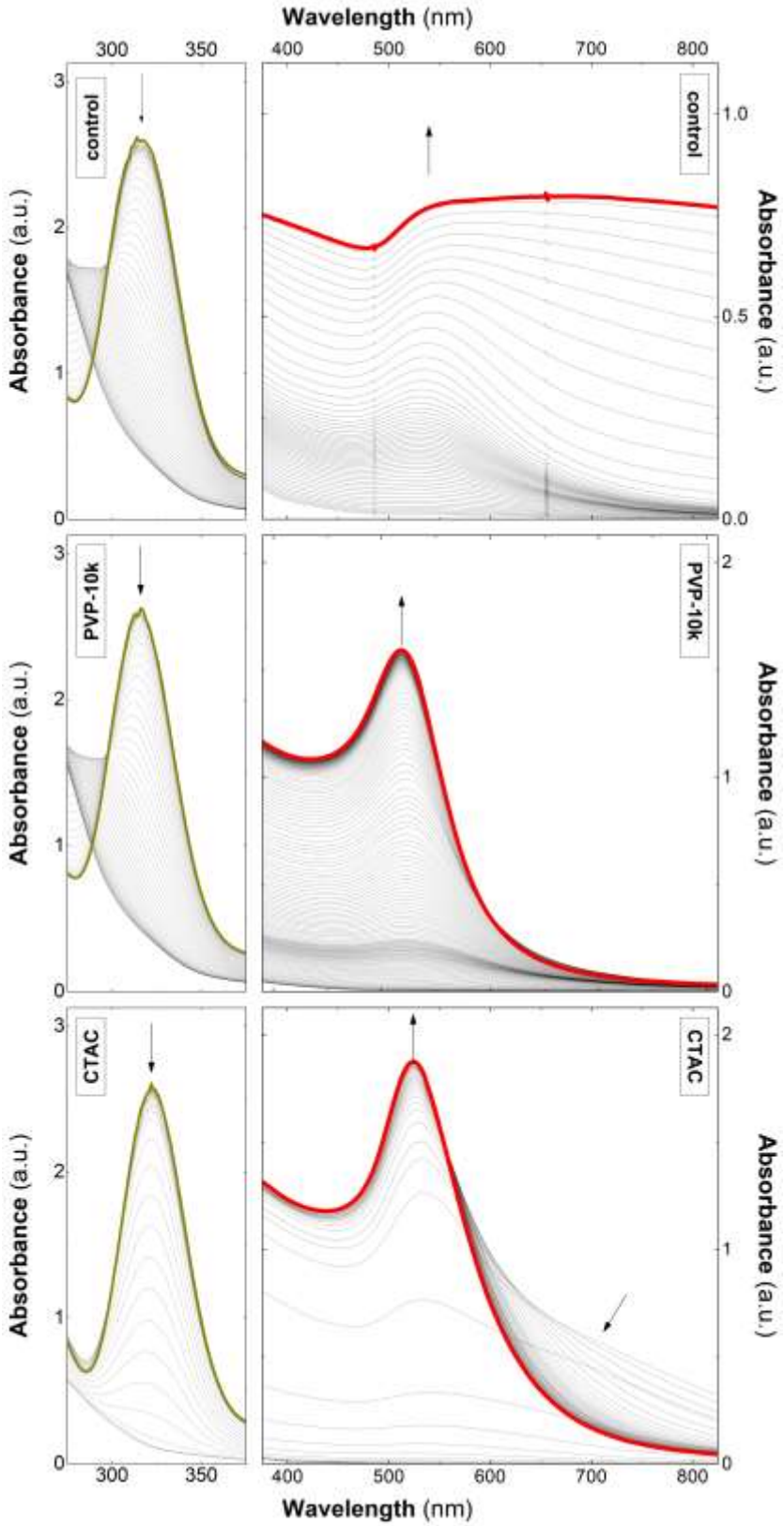

Figure 3. UV-Vis spectra as a function of reaction time (0 to 300 min) for gold reduction mediated by glycidol at 25 °C. The samples were prepared employing initial concentrations of: [$HAuCl_4$] = 0.5 mM, [Cl^-] = 100 mM, [Gly] = 2500 mM (control experiment, upper panel) and [PVP−10k] = 0.11 mM (central panel) or [CTAC] = 10 mM (bottom panel). Arrows indicate the time evolution.

While the reaction proceeds and pH increases, a blue-shift is observed in the maximum position of Au(III) in PVP−10k solution; this behaviour was also observed in solutions containing $HAuCl_4$ and KCl without stabilizing agents (control). This continuous shift is related to the substitution of Cl^- by OH^- in $Au(OH)_xCl_{4-x}^-$ moieties, with $0 \leq x \leq 4$ (see Figure S5), as was reported for titration experiments in which total ligand exchange was achieved.[46] The rate of decay of Au(III) moieties and the subsequent growth of Au nanoparticles are practically identical in the presence or absence of PVP (see figure S6;). Once approximately 20 % of gold has been reduced to the metallic state, dramatic differences between the PVP sample and the control are observed. While the former develops a constant rate growth, the later exhibits an accelerated profile until 60% percent of reduction. At this value, quantitative aggregation and flocculation takes place with the subsequent absorbance decay.

Marked differences are observed for both Au(III) and AuNP regions when alkalinization develops in the presence of CTAC. First, a red-shift of *ca* 8 nm for the maximum position of Au(III) is registered for the initial solution containing CTAC. This suggests that the complex between Au(III) and CTAC (from here Au(III)-CTAC) is present in these experimental conditions.[47] However, maximum position of Au(III)-CTAC remains practically invariant during its consumption showing a higher stability of this complex/moieties over OH^- substitution. Although experimental conditions remain constant, and only changes in the nature of stabilizing agent were induced, a clear change in the AuNP growth mechanism results. Looking at the 375 − 825 nm region, a continuous red-shift of the LSPR maximum during AuNP growth when PVP-10k is used, in good agreement with a process that involves the nucleation of nanospheres that increase their size along the reaction. However, when CTAC is used, the behaviour is essentially different: a blue-shift is observed, matching with a narrowing in the LSPR band. These inherent differences are compiled in Figure S7, that presents the mentioned shifts in the maximum position of $Au(OH)_xCl_{4-x}^-$, Au(III)-CTAC absorption band and LSPR position band of AuNP as a function of reaction time. Beyond the inherent differences between their growth mechanisms, both reactions are completed in terms of Au(III) consumption and the obtained AuNP present a highly symmetric and narrow LSPR bands around 518 nm and 523 nm for PVP-10K and CTAC respectively. Even so, kinetic growth of AuNP is essentially different, i.e., around 2 − 3 times faster when CTAC in employed.

In the search of a detailed morphological characterization of these different growth scenarios, SAXS patterns were recorded during the reaction, in order to model the AuNP size and shape evolution. In this point, it is important to highlight that, due to the strict control in the reaction rate given by the homogeneous alkalinization, several SAXS patterns can be easily obtained, allowing a proper *in situ* isothermal study of the growth kinetics.[48,49] A set of SAXS curves obtained at representative times

10.1002/chem.201905335

for PVP−10k and CTAC samples are presented in Figure 4. Based on the TEM size distribution analysis that showed monomodal histograms for both systems, a non-interactive polydisperse ellipsoid of revolution nanoparticle model[50] was chosen. This model takes into account the anisotropic particle shape and allows performing a proper fitting of each individual pattern (see Appendix in SI). In this particular case, a morphology parameter (ϵ) that accounts for the aspect ratio between the equatorial and axial diameters was defined. For the number size distribution, a non-symmetric Schulz-Zimm[51] normalized distribution was used which allows the inclusion of a polydispersity function with a variance (σ) around a size average diameter (D).[52] In the case of CTAC system, the specific contribution of the micelles was taken into account in the analysis (see Figure SA1).

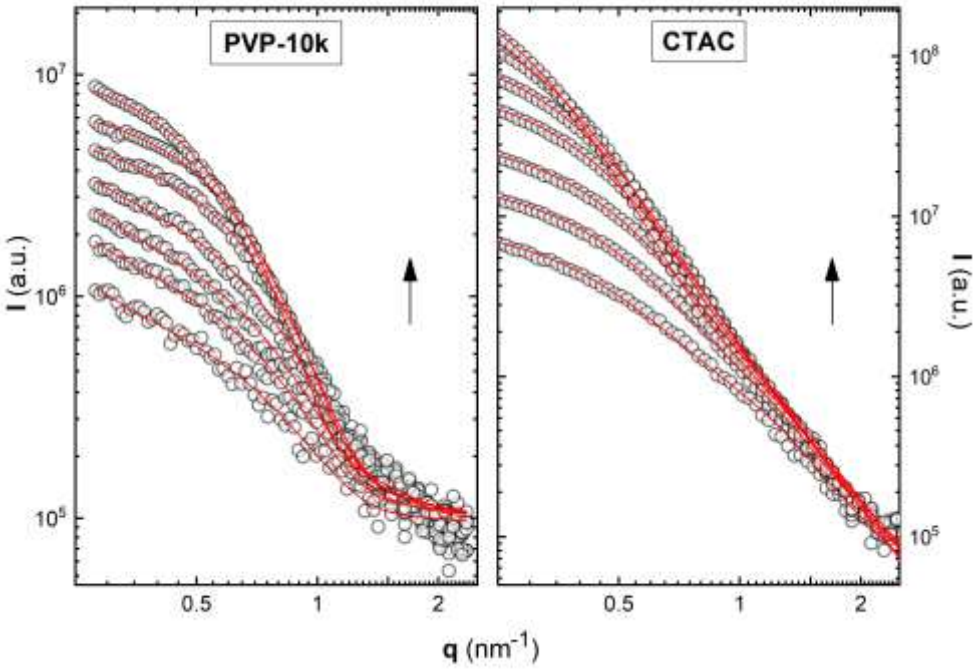

Figure 4. Evolution of SAXS patterns with time (0 to 300 min) and its fitting (red line), for solutions prepared employing initial concentrations of: [$HAuCl_4$] = 0.5 mM, [Cl^-] = 100 mM, [Gly] = 2500 mM and [PVP 10k] = 0.11 mM (left) or [CTAC] = 10 mM (right) at 25 ºC. Arrows indicate time evolution.

For PVP-10k sample, the average diameter after three hours of reaction results in 8 nm with a 2 nm size distribution variance (see Table 1). PVP−10k stabilized AuNP can be modelled as a spherical object ($\epsilon \sim 1$) with a diameter that slightly increases after first detection, LSPR band position measurements support this observation. In the case of CTAC sample, the best fit of the SAXS patterns is obtained when an oblate ellipsoid of revolution is assumed ($\epsilon < 1$). The growth curve shows that during the initial stages AuNP present a highly anisotropic aspect ratio of *ca* 0.45 until they reach the maximum size/volume. Close to the end of this first 20 minutes-long step of reduction and growth, the

10.1002/chem.201905335

nanoparticles develop a maturation process and after 60 minutes the anisotropic aspect ratio increases its value to 0.73 of reaction.

It is important to remark that, for both families of final particles, diameters obtained by SAXS pattern modelling are in close agreement with TEM observations. However, spherical and spheroidal particles with these diameters cannot be distinguished by conventional TEM measurements and/or the maximum position in UV-Vis spectra. SAXS analysis supports the observation of other techniques about the influence of the two stabilizing agents during nanoparticle's nucleation and growth. Moreover, the blue-shift observed in UV-Vis spectra after nucleation for CTAC stabilized samples could be attributed to the nucleation of highly anisotropic nanoparticles ($\epsilon \sim 0.45$) which evolve later into more symmetrical spheroids along the growth process ($\epsilon \sim 0.73$). Table 1 compiles the model's parameters values obtained by non-linear square fit of the experimental SAXS patterns for an *ex situ* experiment performed after three hours of reaction. The values obtained from the volume size distribution are in accordance with TEM size histograms, due to the stronger incidence of the larger particles on the scattered intensity. All reported values correspond with the volume size distribution.

Table 1. size parameters obtained from SAXS fitting. $\boldsymbol{D_{av,N}}$ corresponds to the ellipsoid's average equatorial diameter, σ to the Schulz-Zimm variance for number (N) or volume (V) size distribution function and ϵ to the aspect parameter defined as the ratio between the equatorial and axial diameter.

Stabilising agent	$\boldsymbol{D_{av,N}}$ **nm**	$\boldsymbol{\sigma_N}$	$\boldsymbol{\epsilon}$	$\boldsymbol{D_{av,V}}$ **nm**	$\boldsymbol{\sigma_V}$
PVP-10k	6.2 ± 0.1	1.2	0.98 ± 0.03	8.0 ± 0.1	1.6
CTAC	13.3 ± 0.1	3.9	0.73 ± 0.01	16.6 ± 0.1	4.9

In order to further understand the reaction steps, pH evolution was also assessed; Figure 5 compiles this information along with the rate of Au(III) consumption and reduction into metallic form (AuNP growth) estimated form UV-Vis spectra analysis, and diameters evolution obtained by SAXS fitting. For both CTAC and PVP-10k experiments, as soon the reaction between chloride and Gly takes place, the pH increases from the acid condition given by $HAuCl_4$ up to the most alkaline condition that the present method typically reaches, close to a pH value of 11.[32]

10.1002/chem.201905335

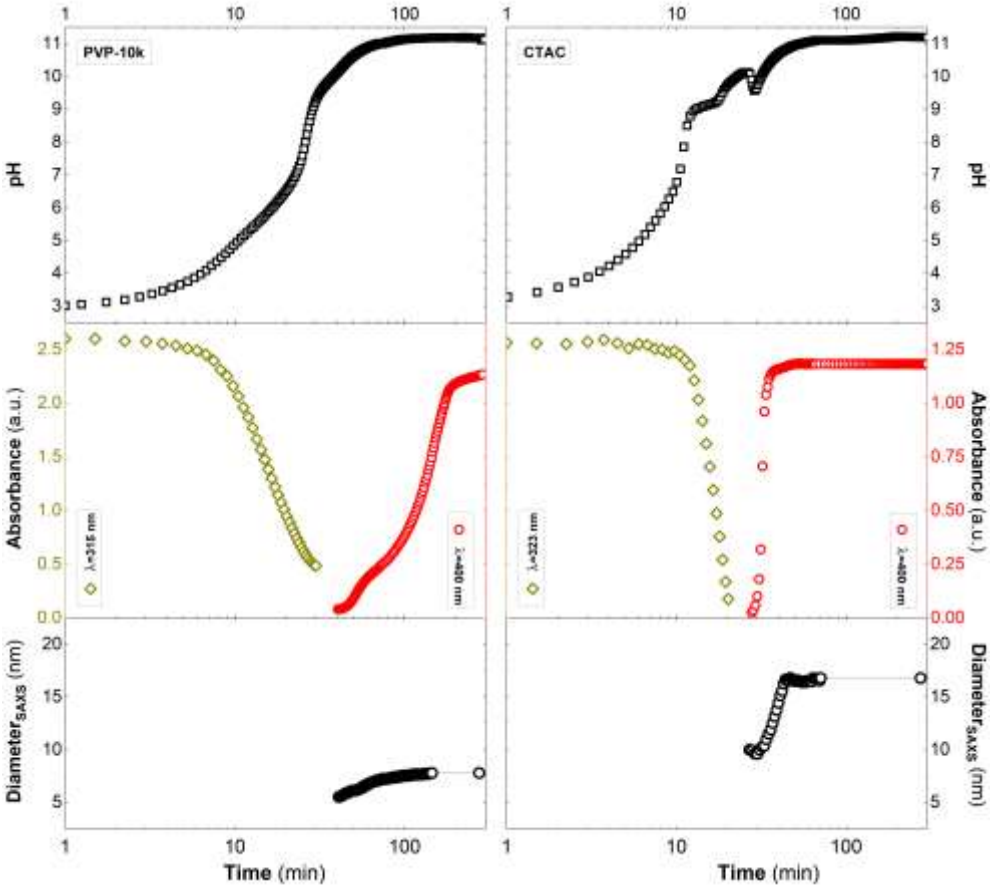

Figure 5. Evolution of pH (upper panel); Au(III) and Au^0 UV-vis traces (central panel) and diameter from SAXS analysis (lower panel) of AuNP employing PVP−10k (left) and CTAC (right). The samples were prepared employing initial concentrations of: [$HAuCl_4$] = 0.5 mM, [Cl^-] = 100 mM, [PVP−10k] = 0.11 mM (left), [CTAC] = 10 mM (right) and [Gly] = 2500 mM at 25 ºC.

The reduction in the presence of PVP takes place with a monotonous increment of pH; nucleation of metallic gold takes place at pH value of 10.0. No pH drops were observed along the nucleation and growth of the metallic phase; having in mind that Au(III) does not form any complex with PVP−10k, the gold complexes distribution, $Au(OH)_xCl_{4-x}^-$, will be modulated by pH exclusively. Then, highly hydroxylated Au(III) species prevail, proving the necessary OH^- equivalents (one per electron) to drive the redox process (see Scheme S1). When Au(III) is reduced in the presence of CTAC, the pH profile presents abrupt changes in its shape. The first deceleration of pH around pH ≈ 9.0 is coincident with the sudden and massive absorption decay of the initially prevalent Au(III)-CTAC complex, to give rise to an intermediate moiety. Once a pH value of ≈ 9.5 is reached, the OH^- consumption of this first step ends and the pH curve's slope increases. At a value of pH ≈ 10.2, a sudden pH-drop overlaps with the birth of AuNP, in agreement with UV-Vis and SAXS inspection, suggesting the occurrence of a nucleation overshoot. In this moment, the AuNP diameter is about half of the final one, which is achieved some minutes afterwards. This second marked acidification can be interpreted in terms of sudden consumption of hydroxyl groups required for

the oxidation of alcohol groups to aldehydes and/or acids (see Scheme S1). The differences in pH values where the reaction takes place when comparing with CTAC experiments, alert about modification in gold species thermodynamic stability mediated by Au(III)−CTAC complex formation. When both CTAC and PVP experiments where repeated employing a lower initial concentration of glycidol (1000 mM), identical pH profiles were observed, indicating the occurrence of a similar sequence of chemical events or reduction mechanism (see Figure S8-S10); for each system, the overall alkalinization/reduction rates were proportionally reduced, according to equation 4.

In summary, by means of a comprehensive characterization, it was demonstrated that two different mechanisms are involved in the AuNP formation mediated by the epoxide route, depending on the nature of the employed stabilizing agent. This study was possible thanks to the fact that the epoxide decomposition is homogeneous and progressively generates the ideal medium for Au(III) reduction, along a time scale fully compatible with a the most commonly employed techniques in kinetic measurements.

3. Kinetics of Au(III) reduction in a sol-gel transition scenario and Hydrogel stabilization. Towards composites on *one-pot* approach. In addition to the explored strategies to stabilize the growing AuNP, a complementary approach was evaluated, taking advantage of the mild alkalinization conditions employed herein. In principle the AuNP formation can be combined with other pH driven chemical transformations, including sol-gel transitions; hydrogels are able to physically trap nanoparticles preventing their aggregation/decantation. By coupling reduction and gelation, composite materials can be prepared through a *one-pot* approach. In this sense, there is a wide pH window before gold reduction/agglomeration takes place, along which several inorganic matrices as Zr(IV),[53] Al(III)[54] or Si(IV)[40] based hydrogels be formed and consolidated, driven by the epoxide route-alkalinization. Since these phases nucleate and quantitatively grow under relatively acidic conditions, their formation can eventually take place before or along gold reduction, allowing the growth of a composite either in a sequential or simultaneous fashion. In order to illustrate this concept, a set of Al(III)-based hydrogel were prepared in the presence of increasing concentrations of $HAuCl_4$, without adding any soluble stabilizing agent. To this aim, both the solvent and the epoxide concentration were modified according to our previous development of high optical quality hydrogels.[53] Figure 6 depicts the evolution of pH and conductivity as well as the main UV-Vis absorption signals belonging to the starting Au(III) precursors and the resultant AuNP. Since the most important contribution to the overall conductivity of the starting solution comes from the $AlCl_3$, the conductivity decay offers a robust indication of the extent of hydroxylation/gelation of $Al(OH)_3$ that drives the sol-gel transition. Between 1 and 30 min, a noticeable drop in the conductivity coexists with an alkalinization plateau centred at a pH value of 3.0, governed by the hydroxylation of Al(III) moieties. Along this step, the sol-gel transition takes place while the concentration of Au(III) soluble precursors

10.1002/chem.201905335

remains almost unaltered. Subsequently, once Al(III) is quantitatively consumed, evidenced by a conductivity decay of almost 90%, pH rises at a faster rate and when a value of 6 is reached, nucleation of gold takes place and quantitative reduction is observed. The decrease on the nucleation pH can be interpreted in terms of a more reducing media employed herein (due to the higher initial Gly concentration) and/or the eventual role of $Al(OH)_3$ surface favouring an heterogenous nucleation process. UV-Vis spectra evidenced an increasing in the intensity of the LSPR band, centred at 530 nm, denoting a similar growth mechanism as observed in the control experiment in the absence of stabilizing agents (see Figure 3). In this case, the lack of specific shifts associated to nanoparticle aggregation, even for the highest Au(III) concentration tested, suggests the growth of AuNP within the microstructure of the hydrogel, avoiding their migration. Beyond these mechanistic aspects, it is worth to mention that the $Al(OH)_3$ hydrogel has a neglectable contribution to the absorption signal along the whole sol-gel and reduction process, as was observed before for related systems, such as nano-ZrO_2 hydrogels.[53] TEM images (Figure 6c) demonstrate that the obtained AuNP are isolated, with spheroidal shape and with an average diameter of 20 nm. This set of experiences demonstrate that the *one-pot* confined growth developed herein provides a suitable strategy for the preparation of stable dispersions of metallic nanoparticles embedded into inorganic matrices through a *one-pot* method, giving rise to a vast plethora of composites. The optimization of the alkalization condition allows the consolidation of a composite containing *"naked"* nanoparticles resulting promising, for example, for catalytic applications.[55]

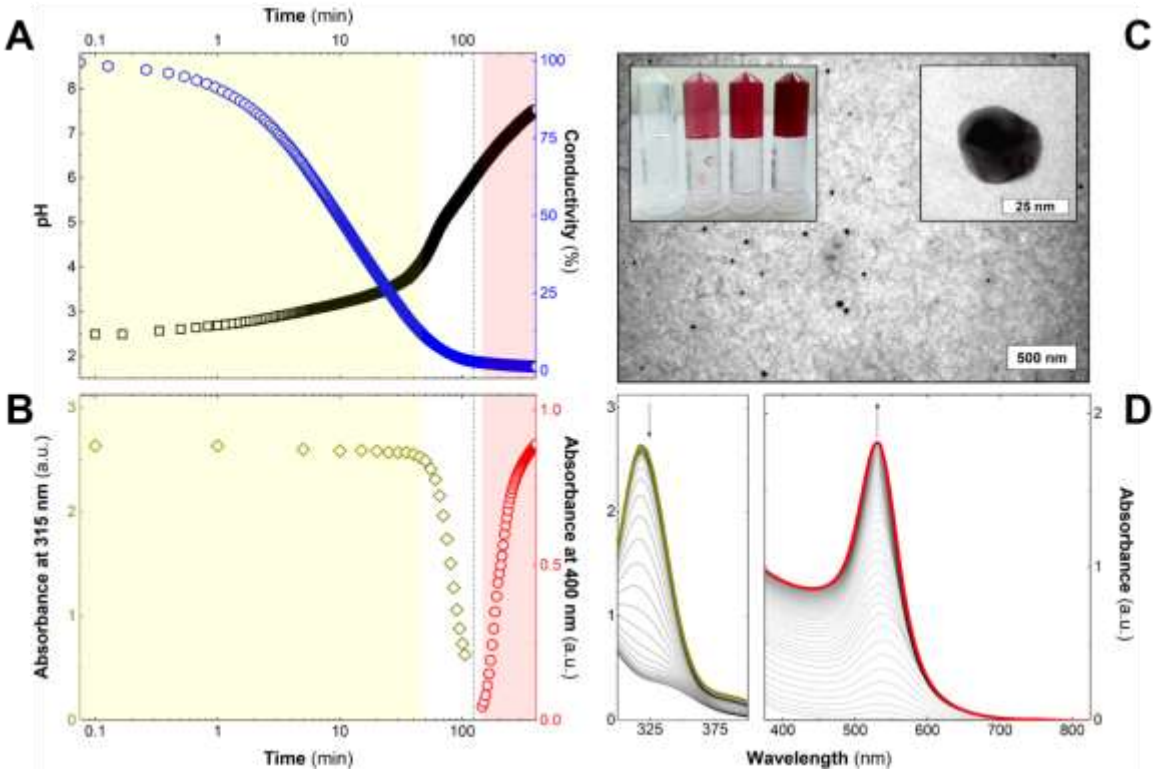

10.1002/chem.201905335

Figure 6. A. Evolution of pH, conductivity, and absorbance (at 315 and 400 nm) for Glycerol:Water solutions (50 % in volume) containing initial concentrations of: $[HAuCl_4]$ = 0.5 mM, $[AlCl_3]$ = 500 mM and [Gly] = 4400 mM at 25 ºC. **B.** Absorbance values recorded at 315 nm and 400 nm are used to follow overall consumption of $Au(OH)_xCl_{4-x}^-$ complexes (yellow zone) and AuNP formation (red zone), respectively; dashed line denotes gelation time. **C.** Digital image of the resulting $Al(OH)_3$ hydrogels hosting the grown Au nanoparticles prepared with $[HAuCl_4]$= 0, 0.25, 0.50 or 1.0 mM; TEM image of the composite sample with $[HAuCl_4]$= 0.5 mM aged for 1000 min. **D.** UV-Vis spectra of the hydrogel as a function of reaction time (t=0 min in yellow, t=1000 min in red); arrows indicate time evolution.

Conclusions

In conclusion, a new methodology to obtain AuNP based on the homogeneous alkalinization through the epoxide route was presented. The proposed method takes advantage of the controlled and simultaneous generation of OH^- and polyol moieties in the reaction medium, until a pH condition is reached in which Au(III) is quantitatively reduced in the form of pure spheroidal AuNP. A stabilizing agent is required to maintain the AuNP suspension, the presence of which dramatically affects the mechanism of growth, resulting in changes in the final particle shape and size, as demonstrated by the evolution of UV-Vis absorption spectra, pH and SAXS patterns. Interestingly, the proposed methodology offers a convenient scenario to follow the reductive species concentration during the reaction (i.e. pH evolution), a feature that is not easily achievable for literature methods. This opens up the possibility for fundamental studies concerning AuNP nucleation and growth in several conditions, and also other metal nanoparticles such as palladium or platinum, among others.

Beyond the inherent kinetic and mechanistic aspects previously discussed, the present synthesis path has certain advantages over other well-established methods. The proposed homogeneous methodology is compatible with the preparation of a wide variety of oxides and hydroxides phases, that effectively stabilize the growing AuNP; these systems are also accessible to implement a comprehensive *in situ* inspection with the aforementioned techniques.

The inherently mild conditions employed allow the addition of thermally labile molecules, opening up the possibility of obtaining key functional materials, ranging from nanocomposites to bio-capped AuNP, in a single *one-pot* approach.

Acknowledgements

This work was supported by the University of Buenos Aires (UBA-CyT 20020130100610BA), the Agencia Nacional de Promoción Científica y Tecnológica (PICT 2015-0351, 2015-3526, 2017-4651), the National Research Council of Argentina (CONICET PIP 11220110101020) and the LNLS (proposal 20170163). VO is member of ALN.

Experimental section

Chemicals. Gold(III) chloride trihydrate ($HAuCl_4 \cdot 3H_2O$), aluminium(III) chloride hexahydrate ($AlCl_3 \cdot 6H_2O$), hydrochloric acid (HCl), potassium chloride (KCl), polyvinylpyrrolidone MW=10000 g/mol (PVP-10k), cetyltrimethylammonium chloride (CTAC), glycerol and glycidol (Gly) were supplied by Sigma-Aldrich. All reagents were used without further purification. Deionized water (18 $M\Omega.cm^{-1}$) was used for all preparations.

AuNP synthesis. Typically, AuNP reduction was performed at 25 ◦C. Experiments were carried out mixing filtrated solution in Milli-Q® water adjusted at pH value of 3.0 ± 0.1 with HCl. In all cases the initial concentrations were adjusted to: [$HAuCl_4$] = 0.5 mM, [KCl] = 100 mM, [PVP−10k] = 0.11 mM or [CTAC] = 10 mM, and [Gly] = 250 − 5000 mM. Firstly, $HAuCl_4$, KCl and HCl pH = 3.0 solution were mixed; then stabilizing agent was added under continuous magnetic stirring. Au(III)−CTAC complex formation is denoted by the formation of bright yellow solid. In this last case, it is necessary to wait a few minutes until the opalescent mixture becomes a clear solution.

AuNP growth kinetics. Representative alkalinization curves were registered by *in situ* potentiometric pH measurement in a reactor at 25 ºC under permanent magnetic stirring. The UV-vis spectra were collected by a Shimadzu spectrophotometer set in kinetic mode. Step time was optimized from 0.5 seconds/spectra to 600 seconds/spectra, depending on the experiment.

$Al(OH)_3$ hydrogel-AuNP synthesis. A set of glycerol:water solutions (50 % in volume) containing [$AlCl_3$] = 500 mM, [Gly] = 4400 mM and variable amounts of [$HAuCl_4$] (0, 0.25, 0.50 or 1.0 mM) were aged at 25 ºC for 1000 min. Absorbance values recorded at 315 nm and 400 nm were used to follow overall consumption of $Au(OH)_xCl_{4-x}^-$ complexes and AuNP formation, respectively. Conductivity and proton activity were recorded along the whole gelation process employing the proper conductimetric and potentiometric probes.

AuNP TEM inspection. As prepared AuNP suspensions were centrifuged at 11000 RPM for 15 minutes and resuspended in water two times. Fifteen microliters of these AuNP samples were drop onto a carbon-coated copper grid and left to dry. TEM inspection was performed in a Philips CM200 TEM operating at 180 kV (GM-CAC-CNEA) or a Philips EM 301 TEM operating at 60 kV (CMA, FCEN, UBA). Average sizes and size distribution of the samples were determined by counting at least 100 particles employing ImageJ software.

AuNP Small Angle X-ray Scattering (SAXS) measurements. The SAXS measurements were performed at the DO2A-SAXS1 beamline of the LNLS (Campinas, Brazil) with a 1.544 Å wavelength. A Pilatus 300K detector was used, with 898.39 mm sample to detector distance. SAXS patterns were recorded with exposure times of 20 seconds with 40 seconds of deadtime between measurements. The scattering intensity distributions as a function of scattering momentum transfer q were obtained in the q range between 0.128 to 5.9 nm^{-1}. One-dimensional

10.1002/chem.201905335

curves were obtained by integration of the 2D data employing the program FIT-2D.[56] Measurements were performed at room temperature in a beamline vacuum-tight temperature-controlled X-ray cell for liquids.[57] The SAXS normalized patterns were fitted employing an in-house written program; the model's parameters were obtained for all patterns by mixing random Gaussian perturbation of the non-linear parameters with least square procedure in order to avoid local minimums.[58] More details can be found in the SI.

References

1. Sanchez Dominguez, M.; Rodriguez Abreu, C., Nanocolloids - A Meeting Point for Scientists and Technologists. *Elsevier: Amsterdam* **2016**.
2. Zhao, P.; Li, N.; Astruc, D., State of the Art in Gold Nanoparticle Synthesis. *Coordination Chemistry Reviews* **2013,** *257*, 638.
3. Xia, Y.; Gilroy, K. D.; Peng, H.-C.; Xia, X., Seed-Mediated Growth of Colloidal Metal Nanocrystals. *Angewandte Chemie International Edition* **2017,** *56* (1), 60-95.
4. Carbó-Argibay, E.; Rodríguez-González, B., Controlled Growth of Colloidal Gold Nanoparticles: Single-Crystalline versus Multiply-twinned Particles. *Israel Journal of Chemistry* **2016,** *56* (4), 214-226.
5. Sepúlveda, B.; Angelomé, P. C.; Lechuga, L. M.; Liz-Marzán, L. M., LSPR-based nanobiosensors. *Nano Today* **2009,** *4* (3), 244-251.
6. Ma, X.; He, S.; Qiu, B.; Luo, F.; Guo, L.; Lin, Z., Noble Metal Nanoparticle-Based Multicolor Immunoassays: An Approach toward Visual Quantification of the Analytes with the Naked Eye. *ACS Sensors* **2019,** *4* (4), 782-791.
7. Banholzer, M. J.; Millstone, J. E.; Qin, L.; Mirkin, C. A., Rationally designed nanostructures for surface-enhanced Raman spectroscopy. *Chemical Society Reviews* **2008,** *37* (5), 885-897.
8. Fan, M.; Andrade, G. F. S.; Brolo, A. G., A review on the fabrication of substrates for surface enhanced Raman spectroscopy and their applications in analytical chemistry. *Analytica Chimica Acta* **2011,** *693* (1), 7-25.
9. Dai, Y.; Wang, Y.; Liu, B.; Yang, Y., Metallic Nanocatalysis: An Accelerating Seamless Integration with Nanotechnology. *Small* **2015,** *11* (3), 268-289.
10. Stratakis, M.; Garcia, H., Catalysis by Supported Gold Nanoparticles: Beyond Aerobic Oxidative Processes. *Chemical Reviews* **2012,** *112* (8), 4469-4506.
11. Zhang, Y.; Cui, X.; Shi, F.; Deng, Y., Nano-Gold Catalysis in Fine Chemical Synthesis. *Chemical Reviews* **2012,** *112* (4), 2467-2505.
12. Liu, L.; Corma, A., Metal Catalysts for Heterogeneous Catalysis: From Single Atoms to Nanoclusters and Nanoparticles. *Chemical Reviews* **2018,** *118* (10), 4981-5079.
13. Dreaden, E. C.; Alkilany, A. M.; Huang, X.; Murphy, C. J.; El-Sayed, M. A., The golden age: gold nanoparticles for biomedicine. *Chemical Society Reviews* **2012,** *41* (7), 2740-2779.
14. Cobley, C. M.; Chen, J.; Cho, E. C.; Wang, L. V.; Xia, Y., Gold nanostructures: a class of multifunctional materials for biomedical applications. *Chemical Society Reviews* **2011,** *40* (1), 44-56.
15. Sperling, R. A.; Rivera Gil, P.; Zhang, F.; Zanella, M.; Parak, W. J., Biological applications of gold nanoparticles. *Chemical Society Reviews* **2008,** *37* (9), 1896-1908.
16. Howes, P. D.; Rana, S.; Stevens, M. M., Plasmonic nanomaterials for biodiagnostics. *Chemical Society Reviews* **2014,** *43* (11), 3835-3853.
17. García-Lojo, D.; Núñez-Sánchez, S.; Gómez-Graña, S.; Grzelczak, M.; Pastoriza-Santos, I.; Pérez-Juste, J.; Liz-Marzán, L. M., Plasmonic Supercrystals. *Accounts of Chemical Research* **2019,** *52* (7), 1855-1864.
18. Angelomé, P. C.; Liz-Marzán, L. M., Synthesis and applications of mesoporous nanocomposites containing metal nanoparticles. *Journal of Sol-Gel Science and Technology* **2014,** *70* (2), 180-190.
19. Innocenzi, P.; Malfatti, L., Nanoparticles in mesoporous films, a happy marriage for materials science. *Journal of Nanoparticle Research* **2018,** *20* (6), 167.
20. Turkevich, J.; Stevenson, P. C.; Hillier, J., A Study of the Nucleation and Growth Processes in the Synthesis of Colloidal Gold. *Discuss. Faraday Soc.* **1951,** *11*, 55.
21. Frens, G., Controlled Nucleation for the Regulation of the Particle Size in Monodisperse Gold Suspensions. *Nature Physical Science* **1973,** *241* (105), 20-22.
22. Zabetakis, K.; Ghann, W. E.; Kumar, S.; Daniel, M. C., Effect of High Gold Salt Concentrations on the Size and Polydispersity of Gold Nanoparticles Prepared by an Extended Turkevich–Frens Method. *Gold Bulletin* **2012,** *45*, 203-211.
23. Ojea-Jiménez, I.; Bastús, N. G.; Puntes, V., Influence of the Sequence of the Reagents Addition in the Citrate-Mediated Synthesis of Gold Nanoparticles. *The Journal of Physical Chemistry C* **2011,** *115*, 15752-15757.
24. Schulz, F.; Homolka, T.; Bastús, N. G.; Puntes, V.; Weller, H.; Vossmeyer, T., Little Adjustments Significantly Improve the Turkevich Synthesis of Gold Nanoparticles. *Langmuir* **2014,** *30*, 10779-10784.
25. Kettemann, F.; Birnbaum, A.; Witte, S.; Wuithschick, M.; Pinna, N.; Kraehnert, R.; Rademann, K.; Polte, J., Missing Piece of the Mechanism of the Turkevich Method: The Critical Role of Citrate Protonation. *Chemistry of Materials* **2016,** *28* (11), 4072-4081.
26. Ferreira, E. B.; Gomes, J. F.; Tremiliosi-Filho, G.; Gasparotto, L. H. S., One-pot eco-friendly synthesis of gold nanoparticles by glycerol in alkaline medium: Role of synthesis parameters on the nanoparticles characteristics. *Materials Research Bulletin* **2014,** *55*, 131-136.
27. Parveen, R.; Tremiliosi-Filho, G., A step ahead towards the green synthesis of monodisperse gold nanoparticles: the use of crude glycerol as a greener and low-cost reducing agent. *RSC Advances* **2016,** *6* (97), 95210-95219.
28. Gomes, J. F.; Garcia, A. C.; Ferreira, E. B.; Pires, C.; Oliveira, V. L.; Tremiliosi-Filho, G.; Gasparotto, L. H. S., New insights into the formation mechanism of Ag, Au and AgAu nanoparticles in aqueous alkaline media: alkoxides from alcohols, aldehydes and ketones as universal reducing agents. *Physical Chemistry Chemical Physics* **2015,** *17* (33), 21683-21693.

29. Parveen, R.; Ullah, S.; Sgarbi, R.; Tremiliosi-Filho, G., One-pot ligand-free synthesis of gold nanoparticles: The role of glycerol as reducing-cum-stabilizing agent. *Colloids and Surfaces A: Physicochemical and Engineering Aspects* **2019,** *565*, 162-171.
30. Parveen, R.; Gomes, J. F.; Ullah, S.; Acuña, J. J. S.; Tremiliosi-Filho, G., One-pot high-yield synthesis of single-crystalline gold nanorods using glycerol as a low-cost and eco-friendly reducing agent. *Journal of Nanoparticle Research* **2015,** *17* (10), 418.
31. Rodrigues, T. S.; Zhao, M.; Yang, T.-H.; Gilroy, K. D.; da Silva, A. G. M.; Camargo, P. H. C.; Xia, Y., Synthesis of Colloidal Metal Nanocrystals: A Comprehensive Review on the Reductants. *Chemistry – A European Journal* **2018,** *24* (64), 16944-16963.
32. Oestreicher, V.; Jobbágy, M., One pot synthesis of $Mg_2Al(OH)_6Cl \cdot 1.5H_2O$ layered double hydroxides: The epoxide route. *Langmuir* **2013,** *29* (39), 12104-12109.
33. Tarutani, N.; Tokudome, Y.; Jobbágy, M.; Viva, F. A.; Soler-Illia, G. J. A. A.; Takahashi, M., Single-Nanometer-Sized Low-Valence Metal Hydroxide Crystals: Synthesis via Epoxide-Mediated Alkalinization and Assembly toward Functional Mesoporous Materials. *Chemistry of Materials* **2016,** *28* (16), 5606-5610.
34. Tokudome, Y.; Fukui, M.; Tarutani, N.; Nishimura, S.; Prevot, V.; Forano, C.; Poologasundarampillai, G.; Lee, P. D.; Takahashi, M., High-Density Protein Loading on Hierarchically Porous Layered Double Hydroxide Composites with a Rational Mesostructure. *Langmuir* **2016,** *32* (35), 8826-8833.
35. Gash, A. E.; Tillotson, T. M.; Satcher, J. H.; Hrubesh, L. W.; Simpson, R. L., New sol-gel synthetic route to transition and main-group metal oxide aerogels using inorganic salt precursors. *Journal of Non-Crystalline Solids* **2001,** *285* (1-3), 22-28.
36. Arencibia, N.; Oestreicher, V.; Viva, F. A.; Jobbágy, M., Nanotextured alpha Ni(II)-Co(II) hydroxides as supercapacitive active phases. *RSC Advances* **2017,** *7* (10), 5595-5600.
37. Oestreicher, V.; Hunt, D.; Torres-Cavanillas, R.; Abellán, G.; Scherlis, D. A.; Jobbágy, M., Halide-Mediated Modification of Magnetism and Electronic Structure of α-Co(II) Hydroxides: Synthesis, Characterization, and DFT+U Simulations. *Inorganic Chemistry* **2019,** *58* (14), 9414-9424.
38. Oestreicher, V.; Fábregas, I.; Jobbágy, M., One-pot epoxide-driven synthesis of $M_2Al(OH)_6Cl \cdot 1.5H_2O$ layered double hydroxides: Precipitation mechanism and relative stabilities. *Journal of Physical Chemistry C* **2014,** *118* (51), 30274-30281.
39. Tokudome, Y.; Morimoto, T.; Tarutani, N.; Vaz, P. D.; Nunes, C. D.; Prevot, V.; Stenning, G. B. G.; Takahashi, M., Layered Double Hydroxide Nanoclusters: Aqueous, Concentrated, Stable, and Catalytically Active Colloids toward Green Chemistry. *ACS Nano* **2016,** *10* (5), 5550-5559.
40. Tillotson, T. M.; Sunderland, W. E.; Thomas, I. M.; Hrubesh, L. W., Synthesis of lanthanide and lanthanide-silicate aerogels. *Journal of Sol-Gel Science and Technology* **1994,** *1* (3), 241-249.
41. Tokudome, Y.; Miyasaka, A.; Nakanishi, K.; Hanada, T., Synthesis of hierarchical macro/mesoporous dicalcium phosphate monolith via epoxide-mediated sol-gel reaction from ionic precursors. *Journal of Sol-Gel Science and Technology* **2011,** *57* (3), 269-278.
42. Oestreicher, V.; Jobbágy, M., Extremely efficient crystallization of HKUST-1 and Keggin-loaded related phases through the epoxide route. *Chemical Communications* **2017,** *53* (24), 3466-3468.
43. Hendel, T.; Wuithschick, M.; Kettemann, F.; Birnbaum, A.; Rademann, K.; Polte, J., In Situ Determination of Colloidal Gold Concentrations with UV–Vis Spectroscopy: Limitations and Perspectives. *Anal. Chem.* **2014,** *86* (22), 11115-11124.
44. Peck, J. A.; Tait, C. D.; Swanson, B. I.; Brown, G. E., Speciation of aqueous gold(III) chlorides from ultraviolet/visible absorption and Raman/resonance Raman spectroscopies. *Geochimica et Cosmochimica Acta* **1991,** *55* (3), 671-676.
45. Noguez, C., Surface Plasmons on Metal Nanoparticles: The Influence of Shape and Physical Environment. *The Journal of Physical Chemistry C* **2007,** *111* (10), 3806-3819.
46. Usher, A.; McPhail, D. C.; Brugger, J., A spectrophotometric study of aqueous Au(III) halide–hydroxide complexes at 25–80°C. *Geochimica et Cosmochimica Acta* **2009,** *73* (11), 3359-3380.
47. Rodríguez-Fernández, J.; Pérez-Juste, J.; Mulvaney, P.; Liz-Marzán, L. M., Spatially-Directed Oxidation of Gold Nanoparticles by Au(III)−CTAB Complexes. *The Journal of Physical Chemistry B* **2005,** *109* (30), 14257-14261.
48. Pschunder, F.; Puig, J.; Giovanetti, L. J.; Huck-Iriart, C.; Requejo, F. G.; Buceta, D.; Hoppe, C. E.; Ramallo-López, J. M., New Insights into the Growth Mechanism of Ultrathin Au Nanowires from Combined in Situ EXAFS and SAXS Studies. *The Journal of Physical Chemistry C* **2018,** *122* (50), 29051-29061.
49. Tarutani, N.; Tokudome, Y.; Jobbágy, M.; Soler-Illia, G. J. A. A.; Tang, Q.; Müller, M.; Takahashi, M., Highly Ordered Mesoporous Hydroxide Thin Films through Self-Assembly of Size-Tailored Nanobuilding Blocks: A Theoretical-Experimental Approach. *Chemistry of Materials* **2019,** *31* (2), 322-330.
50. Pedersen, J. S., Analysis of small-angle scattering data from colloids and polymer solutions: modeling and least-squares fitting. *Advances in Colloid and Interface Science* **1997,** *70*, 171-210.
51. Zimm, B. H., The Scattering of Light and the Radial Distribution Function of High Polymer Solutions. *The Journal of Chemical Physics* **1948,** *16* (12), 1093-1099.
52. Huck-Iriart, C.; Montes-de-Oca-Ávalos, J.; Herrera, M. L.; Candal, R. J.; Pinto-de-Oliveira, C. L.; Linares-Torriani, I., New insights about flocculation process in sodium caseinate-stabilized emulsions. *Food Research International* **2016,** *89*, 338-346.
53. Oestreicher, V.; Perullini, M.; Jobbágy, M., Physicochemical aspects of epoxide driven nano-ZrO_2 hydrogel formation: Milder kinetics for better properties. *Dalton Transactions* **2016,** *45* (24), 9920-9924.

54. Tokudome, Y.; Nakanishi, K.; Kanamori, K.; Hanada, T., In situ SAXS observation on metal-salt-derived alumina sol-gel system accompanied by phase separation. *Journal of Colloid and Interface Science* **2010,** *352* (2), 303-308.
55. Bastús, N. G.; Merkoçi, F.; Piella, J.; Puntes, V., Synthesis of Highly Monodisperse Citrate-Stabilized Silver Nanoparticles of up to 200 nm: Kinetic Control and Catalytic Properties. *Chemistry of Materials* **2014,** *26* (9), 2836-2846.
56. Hammersley, A., FIT2D: a multi-purpose data reduction, analysis and visualization program. *Journal of Applied Crystallography* **2016,** *49* (2), 646-652.
57. Cavalcanti, L. P.; Torriani, I. L.; Plivelic, T. S.; Oliveira, C. L. P.; Kellermann, G.; Neuenschwander, R., Two new sealed sample cells for small angle x-ray scattering from macromolecules in solution and complex fluids using synchrotron radiation. *Review of Scientific Instruments* **2004,** *75* (11), 4541-4546.
58. da Silva Costa, D.; Huck-Iriart, C.; Kellermann, G.; Giovanetti, L. J.; Craievich, A. F.; Requejo, F. G., In situ study of the endotaxial growth of hexagonal $CoSi_2$ nanoplatelets in Si(001). *Appl. Phys. Lett.* **2015,** *107* (22), 223101.